

Distributed Hammerstein Modeling for Cross-Coupling Effect of Multiaxis Piezoelectric Micropositioning Stages

Hai-Tao Zhang , Senior Member, IEEE, Bo Hu, Linlin Li, Zhiyong Chen , Senior Member, IEEE, Dongrui Wu , Senior Member, IEEE, Bowen Xu, Xiang Huang, Guoying Gu , Member, IEEE, and Ye Yuan , Member, IEEE

Abstract—Hysteresis modeling is interesting yet challenging for piezoelectric actuated systems, which are often used in micro/nano scale measurement and manufacturing equipments. However, due to its complexity, few efforts have been devoted to characterizing cross-coupling hysteresis effect of multiaxis piezoelectric micropositioning stages. To this end, a distributed Hammerstein model, composed of a cascaded connection of a static nonlinearity and a dynamic linearity, is proposed in this paper to approximate the nonlinear spatial/temporal cross-coupling effect. This model outperforms conventional piezo models, such as the Preisach model. Meanwhile, theoretical analysis is provided to guarantee the convergence of the proposed Hammerstein model. Finally, extensive experiments are conducted to verify the superiority of the proposed modeling method.

Index Terms—Hysteresis, modeling, piezoelectric devices.

I. INTRODUCTION

THESE years have witnessed the tremendous development of nanopositioning systems widely used in modern nanometer measurement and manufacturing equipments. To obtain high precision of nanoscale positioning systems, like scanning tunneling microscopes (STMs) [1], atomic force

microscopes (AFMs) [2], lithographic machines [3], ultrahigh vacuum precise positioning devices [4], microrobot arm [5], etc., smart material actuators, represented by piezoelectric actuators [6]–[8], are commonly used.

The positioning control precision of piezoelectric actuators is bottlenecked by the nonlinear dynamics including creep and hysteresis. Recently, the adverse effects of cross couplings of multiaxis piezoelectric micropositioning stages have attracted more and more attentions [9]. Take AFMs, for example, *triangular signals* applied to the X -piezoelectric actuated scanner often deform the trajectory in the X - Y landscape and hence distorts the scanned images due to the X - Y axes cross-coupling effect [10]. Significantly, the cross-coupling effect is dominant at high frequencies, which may cause not only crumpling and tilting the scans [10], [11], but also the loss of the surface information about the sample [12]. Such a nonnegligible cross-coupling effect mainly caused by interaxis friction, pressure, and preload forces substantially lowers the positioning control precision. Thus, the cross-coupling effect becomes one of the main complications associated to micro/nano scale detection processes (e.g., AFMs and STMs) and nano-manufacturing equipments (e.g., lithographic machines). However, due to its complex cross-axis dynamics, most of the existing modeling schemes, including Preisach [13], Bouc–Wen [14], Prandtl–Ishlinskii [15], cascaded nonlinearity [6] models, merely focus on the single-axis hysteresis dynamics.

Till date, there are very few niche modeling methods for cross-coupling hysteresis of the multiaxis piezoelectric micropositioning stages, which are however indispensable for both piezoelectric actuated mechanism analysis and high-precision controller design. Most of the existing works [9], [11], [16], [17] focused on decoupling the cross couplings to facilitate controller design. For instance, Yong *et al.* [9] developed a robust H_∞ controller to minimize the X - Y axes cross coupling of the piezoelectric actuated stage of an AFM. Habibullah *et al.* [11] designed an internal reference model-based optimal linear quadratic Gaussian (LQG) controller to address the cross-coupling effect of a high-precision lateral positioning used in a piezoelectric tube scanner (PTS) of an AFM. Wu *et al.* [16] proposed an adaptive double integral sliding mode control scheme to compensate for the cross-coupling in AFMs, where phase feedback signals were used as well to increase the scanning sensitivity. Rana

Manuscript received September 18, 2017; revised February 11, 2018 and June 12, 2018; accepted September 4, 2018. Date of publication September 17, 2018; date of current version December 13, 2018. Recommended by Technical Editor Q. Zou. This work was supported by the National Natural Science Foundation of China under Grant U1713203, Grant 51729501, Grant 61673189, Grant 51535004, Grant 61751303, and Grant 91748112. (Corresponding author: Ye Yuan.)

H.-T. Zhang, B. Hu, B. Xu, D. Wu, X. Huang, and Y. Yuan are with the School of Automation, the State Key Lab of Digital Manufacturing Equipment and Technology, and the Key Lab of Imaging Processing and Intelligence Control, Huazhong University of Science and Technology, Wuhan 430074, China (e-mail: zht@mail.hust.edu.cn; bob_machinist@foxmail.com; xubowenjason@163.com; drwu@hust.edu.cn; huangxiang92@hust.edu.cn; ye.yuan@outlook.com).

L. Li and G. Gu are with the State Key Laboratory of Mechanical System and Vibration, School of Mechanical Engineering, Shanghai Jiao Tong University, Shanghai 200240, China (e-mail: lilinlin321@sjtu.edu.cn; guguoqing@sjtu.edu.cn).

Z. Chen is with the School of Electrical Engineering and Computing, The University of Newcastle, Callaghan NSW 2308, Australia (e-mail: zhiyong.chen@newcastle.edu.au).

Color versions of one or more of the figures in this paper are available online at <http://ieeexplore.ieee.org>.

Digital Object Identifier 10.1109/TMECH.2018.2870864

et al. [17] designed a multi-input multioutput model predictive control (MPC) method to counteract the cross coupling in a PTS.

Among the few existing works of direct identification on cross-coupling hysteresis dynamics, Tan *et al.* [18] developed a neural-network-based sandwich model to describe the nonlinear X - Y axes interactive dynamics, which was afterwards used in a nonlinear decoupling controller to counterbalance the cross-axis coupling effect. Based on the response surface methodology, Qin *et al.* [19] proposed a computational optimization method to address the cross-axis interactive dynamics. With such an optimization method, they presented a novel mechanical design for a 2-DOF piezoelectric actuator to substantially alleviate the cross-axis coupling. With the assistance of laser interferometry sensors, Bhagat *et al.* [20] proposed a parameter identification approach, which was afterwards used in a robust motional controller to compensate for the cross-axis coupling effect between the two axes of a flexure-based stage. Fung *et al.* [21] proposed an improved Bouc–Wen hysteresis model to identify the cross-coupling effects, where a real-coded genetic algorithm method was adopted to train the model parameters. Das *et al.* [22] provided a linear data-driven modeling method to approach the cross-coupling dynamics of a scanner in the lateral and longitudinal axes, which was subsequently used in a negative-imaginary damping controller to restrain the first resonant mode and to attenuate the cross-coupling effect as well. Xu [23] proposed a least square support vector machine learning method, which has gained better modeling performance than traditional Bouc–Wen model [14]. From the modeling aspect of distributed parameter systems, Qi *et al.* [24] proposed a kernel-based modeling scheme with the assistance of Karhunen–Loève decomposition and Galerkin method, which shows the potential of approaching cross-coupling effect of piezoelectrical stage. Li *et al.* [25] and Lai *et al.* [26] adopted a finite element analysis method to investigate the cross-coupling dynamics around the resonance frequency. Accordingly, they designed a center-thickened beam structure together with a symmetric configuration of the parallelogram flexure to effectively reduce the cross-coupling effect. So far, most of the existing cross-coupling modeling methods are either linear or lumping system orientation. Thus, it is still an urgent yet challenging task to develop an effective modeling method to approximate the nonlinear spatial/temporal dynamics of cross-coupling effect of piezoelectric stages.

To fulfill such a task, in this paper, we develop a pure data-driven distributed multichannel Hammerstein model. The present model is a cascade connection of a static nonlinear block and a dynamic spatial/temporal linear block. By feeding a periodical exciting signal to the Y -axis, the spatial/temporal data is gathered at different X - Y axes contacting positions. Accordingly, a multichannel identification scheme is derived to guarantee high modeling precision without any prior knowledge about the midoutput. Afterwards, matrix spectrum analysis is conducted to guarantee the convergence, and the modeling accuracy of the proposed Hammerstein modeling method. Finally, data-driven experimental modeling performances are provided to verify the effectiveness and superiority of the model.

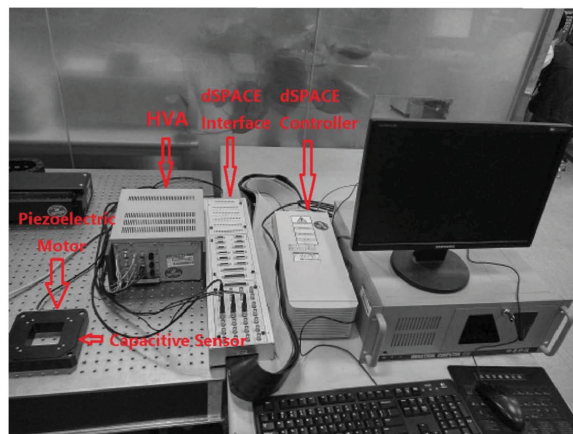


Fig. 1. Physik Instrument (P-563.3CD) two-axis piezoelectric actuated stage.

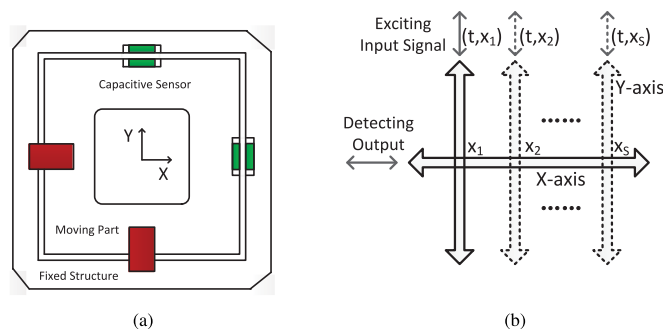


Fig. 2. (a) Schematic map of the piezoelectric stage. (b) Cross coupling between X - Y axis of different X - Y axes contacting positions.

The remainder of the paper is organized as follows. The piezoelectric actuated stage is described in Section II. Then, the distributed Hammerstein modeling scheme is proposed in Section III, and a systematic analysis on the convergence of the scheme is provided as well. Afterwards, extensive modeling experiments are conducted to verify the feasibility and superiority of the proposed Hammerstein model in Section IV. Finally, the conclusion is drawn in Section V.

Throughout the paper, the following notations are used: A^T denotes the transposition of a matrix A , \mathbb{R} , \mathbb{R}^+ , \mathbb{Z} , \mathbb{N} , and \mathbb{C} are real number, positive real number, integers, positive integers, and complex number sets, respectively. The operator \otimes represents the Kronecker product.

II. EXPERIMENTAL PIEZOELECTRIC ACTUATED STAGE

The experimental platform, i.e., a Physik Instrument (PI-563.3CD) two-axis piezoelectric actuated stage (in abbr. PI stage) is shown in Fig. 1 with structure given in Fig. 2. Therein, two piezoelectric actuators and two capacitive position sensors are mounted to the X - and Y -axes, respectively. The resonance frequencies of X - and Y -axes are both 140 Hz. The block diagram of the PI stage is given in Fig. 3, where an exciting signal u is fed into a high-voltage amplifier (HVA) via a digital-to-analog (D/A) converter, where a u_c signal is yielded to drive the PI stage. Then, the X - and Y -axes displacements are measured

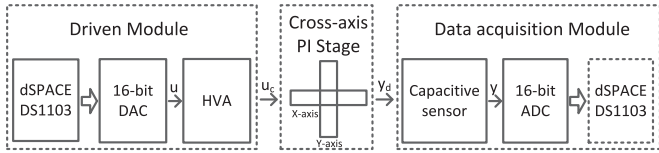


Fig. 3. Block diagram of the PI-stage control system.

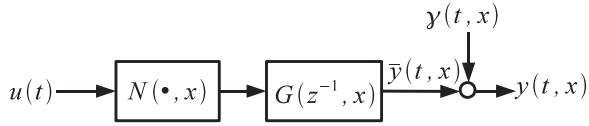


Fig. 4. Distributed Hammerstein model.

by capacitive displacement transducers (CDTs). Afterwards, the displacement signal is transferred to a voltage signal, and then fed into the dSPACE-DS1103 block through an analog-to-digital (A/D) converter.

In Fig. 2(a), due to the preload forces together with the frictions and the asymmetrical structure of the PI-stage, the motions along X - and Y -axes affect each other, which is thus named as the cross-coupling effect. Quantitative analysis confirms that the intensity of cross coupling is nonnegligible for high-precision positioning control scenarios. To investigate such a complex coupling effect, we feed an exciting signal u to Y -axis of the PI-stage at different X - Y axes contacting positions x_i , $i = 1, \dots, S$, and measure the X -axis displacement as shown in Fig. 2(b). Distinct cross couplings are observed at different contacting positions, which induces the nonnegligible adverse spatial/temporal effect of the cross couplings.

III. MODELING METHOD DEVELOPMENT

In this section, we aim to develop a nonlinear Hammerstein model to approximate the spatial/temporal cross-axis dynamics. As shown in Fig. 4, suppose the desired dynamics consists of a cascade connection of a memoryless nonlinearity $N(\cdot, x)$ and a distributed linear block $G(z^{-1}, x)$. More specifically, they are governed by the following the input–output equation:

$$y(t, x) = G(z^{-1}, x) \cdot N(u(t), x) + \gamma(t, x) \quad (1)$$

where $u(t), y(t, x), \gamma(t, x) \in \mathbb{R}$ are the system input, output, and external noise, respectively. The output function $y(t, x)$ represents the X -axis displacement at t when the X - Y axes contacting position is x , as shown in Fig. 2(b).

First, the linear block is assumed to be expanded by a rational orthonormal basis series as follows:

$$G(z^{-1}, x) = \sum_{i=1}^m \rho^T(x) \xi_i L_i(z^{-1}) = [L(z^{-1}) \otimes \rho(x)]^T \xi \quad (2)$$

where $\xi = [\xi_1^T, \dots, \xi_m^T]^T$ and $L(\cdot) = [L_1(\cdot)^T, \dots, L_m(\cdot)^T]^T$, and $L_1(z^{-1}), \dots, L_m(z^{-1})$ form a rational orthonormal basis on the Hardy space $\mathbb{H}(\mathbf{T})$ [27]. For our model, they are set as discrete Laguerre series detailed in the Appendix. The term $\rho^T(x) \xi_i \in \mathbb{R}$, $i = 1, 2, \dots, m$, is the associated coefficient depending on the spatial position x . Specifically, $\rho(\cdot) : \mathbb{R} \mapsto \mathbb{R}^q$

is a known vector function, and $\xi_i \in \mathbb{R}^q$ is a vector parameter to be identified.

Second, the nonlinear block can be described as

$$N(u(t), x) = \sum_{i=1}^n \psi^T(x) \eta_i g_i(u(t)) = [g(u(t)) \otimes \psi(x)]^T \eta \quad (3)$$

where $\eta = [\eta_1^T, \dots, \eta_n^T]^T$, $g(\cdot) = [g_1(\cdot)^T, \dots, g_n(\cdot)^T]^T$, $g_i(\cdot) : \mathbb{R} \mapsto \mathbb{R}$ is a known nonlinear basis function, and $\psi^T(x) \eta_i \in \mathbb{R}$ is its associated coefficient depending on the spatial position x , $i = 1, \dots, n$. Specifically, $\psi(\cdot) : \mathbb{R} \mapsto \mathbb{R}^p$ is a known vector function, and $\eta_i \in \mathbb{R}^p$ is a vector parameter to be identified. Generally speaking, $g_i(\cdot)$ can be chosen as polynomials, radial basis functions (RBF), wavelets, etc. For simplicity, we pick $g_i(\cdot)$ as the polynomial series in our model. Both the functions $\rho(\cdot)$ and $\psi(\cdot)$ can be selected as some basis functions, e.g., polynomials, Jacobies, trigonometric functions, or their combinations.

By (2) and (3), (1) is equivalent to

$$y(t, x) = [L(z^{-1}) \otimes \rho(x)]^T \xi \cdot [g(u(t)) \otimes \psi(x)]^T \eta + \gamma(t, x). \quad (4)$$

Direct calculation leads to

$$\begin{aligned} & [L(z^{-1}) \otimes \rho(x)]^T \xi \cdot [g(u(t)) \otimes \psi(x)]^T \eta \\ &= [L(z^{-1}) \otimes \rho(x)]^T \otimes [g(u(t)) \otimes \psi(x)]^T [\xi \otimes \eta] \\ &= [L(z^{-1}) \otimes \rho(x) \otimes g(u(t)) \otimes \psi(x)]^T [\xi \otimes \eta] \end{aligned}$$

thus, (4) is equivalent to

$$y(t, x) = \phi^T(z^{-1}, u(t), x) \theta + \gamma(t, x) \quad (5)$$

where

$$\phi(z^{-1}, u(t), x) = L(z^{-1}) \otimes \rho(x) \otimes g(u(t)) \otimes \psi(x)$$

is a known vector function and

$$\theta = \xi \otimes \eta$$

is a vector parameter to be identified. For convenience, we denote the noise-free output as

$$\bar{y}(t, x) = \phi^T(z^{-1}, u(t), x) \theta. \quad (6)$$

Next, the modeling procedure is to establish an equation

$$\hat{y}(t, x) = \phi^T(z^{-1}, u(t), x) \hat{\theta} \quad (7)$$

where $\hat{\theta} = \hat{\xi} \otimes \hat{\eta}$ is a valid estimation of θ for some vectors $\hat{\xi}$ and $\hat{\eta}$. This objective is usually impossible when noise appears, so a more realistic model is

$$\hat{y}(t, x) = \phi^T(z^{-1}, u(t), x) \sum_{i=1}^{N_c} \hat{\theta}^{(i)}, \quad \hat{\theta}^{(i)} = \hat{\xi}^{(i)} \otimes \hat{\eta}^{(i)} \quad (8)$$

for an integer $N_c \geq 1$. By using the similar arguments, the model (8) is equivalent to

$$\begin{aligned}\hat{y}(t, x) &= \sum_{i=1}^{N_c} \hat{G}(z^{-1}, x) \cdot \hat{N}(u(t), x) \\ \hat{G}^{(i)}(z^{-1}, x) &= [L(z^{-1}) \otimes \rho(x)]^T \hat{\xi}^{(i)} \\ \hat{N}^{(i)}(u(t), x) &= [g(u(t)) \otimes \psi(x)]^T \hat{\eta}^{(i)}.\end{aligned}\quad (9)$$

Such a model is called a *multichannel Hammerstein model*, and N_c is the number of channels. The objective of this paper is using the given input $u(t)$ with position x and the measured output $y(t, x)$ from (5) (or equivalently (1)), find valid estimation $\hat{\theta}^{(i)} = \hat{\xi}^{(i)} \otimes \hat{\eta}^{(i)}$, $i = 1, \dots, N_c$, such that the output $\hat{y}(t, x)$ determined by the multichannel Hammerstein (8) (or equivalently (9)) matches $\bar{y}(t, x)$ of (6) in a certain sense.

The approach to achieving the aforementioned objective is developed in a rigorous manner as follows. Select an input series $U := [u(t_1), u(t_2), \dots, u(t_N)]$ with temporal variable sequence $\{t_1, t_2, \dots, t_N\}$, and collect the corresponding NS -sampling output spatial/temporal dataset with spatial variable sequence $X := [x_1, x_2, \dots, x_S]$ for two integers $N, S \geq 1$. Thus, the dynamics (5) become

$$Y = \Phi\theta + \Upsilon \quad (10)$$

with

$$\begin{aligned}Y &:= [y(t_1, x_1), y(t_2, x_1), \dots, y(t_N, x_1), \dots, \\ &\quad y(t_1, x_S), y(t_2, x_S), \dots, y(t_N, x_S)]^T \\ \Phi &:= [\phi(z^{-1}, u(t_1), x_1), \dots, \phi(z^{-1}, u(t_N), x_1), \dots, \\ &\quad \phi(z^{-1}, u(t_1), x_S), \dots, \phi(z^{-1}, u(t_N), x_S)]^T \\ \Upsilon &:= [\gamma(t_1, x_1), \gamma(t_2, x_1), \dots, \gamma(t_N, x_1), \dots, \\ &\quad \gamma(t_1, x_S), \gamma(t_2, x_S), \dots, \gamma(t_N, x_S)]^T.\end{aligned}$$

Then, the following two steps are applied: 1) find a valid estimation $\hat{\theta}$ of θ through the data Φ and Y , depending on U and X ; and 2) derive the multiple channel estimation $\hat{\theta}^{(i)} = \hat{\xi}^{(i)} \otimes \hat{\eta}^{(i)}$, $i = 1, \dots, N_c$, from $\hat{\theta}$ to fit in the multichannel Hammerstein model (8).

To elaborate the two steps, we first define a function $\mathcal{C}(\cdot)$ such that

$$\hat{\Theta} = \mathcal{C}^{-1}(\hat{\theta}) \in \mathbb{R}^{n_p \times m_q}, \quad \hat{\theta} = \mathcal{C}(\hat{\Theta}) \in \mathbb{R}^{n_p m_q}$$

where the vector $\hat{\theta}$ is the block column matrix of $\hat{\Theta}$, i.e., stacking the block column of $\hat{\Theta}$ on the top of each other. Then, we give a result on the singular value decomposition (SVD) of a matrix with rank deficiency.

Theorem 3.1: ([28, Th. 2.5.3]) Let the SVD of the matrix $\hat{\Theta} \in \mathbb{R}^{s_1 \times s_2}$ with $\text{rank}(\hat{\Theta}) = k \geq 1$ be given as $\hat{\Theta} = W\Sigma V^T$ where

$$\begin{aligned}W &= [w_1, \dots, w_{s_1}] \in \mathbb{R}^{s_1 \times s_1} \\ V &= [v_1, \dots, v_{s_2}] \in \mathbb{R}^{s_2 \times s_2}\end{aligned}\quad (11)$$

are orthogonal matrix and

$$\begin{aligned}\Sigma &= \text{diag}\{\sigma_1, \dots, \sigma_s\} \in \mathbb{R}^{s_1 \times s_2}, \quad s = \min\{s_1, s_2\} \\ \sigma_1 &\geq \sigma_2 \geq \dots \geq \sigma_k > \sigma_{k+1} = \dots = \sigma_s = 0.\end{aligned}$$

Then, for $0 \leq l \leq k$

$$e^{(l)} := \left\| \hat{\Theta} - \sum_{i=1}^l \sigma_i w_i v_i^T \right\|_2 = \sigma_{l+1}.$$

N.B. if $k = s$, we denote $\sigma_{s+1} = 0$ for the completeness of notation.

The main technical result is stated in the following theorem.

Theorem 3.2: For the distributed system (1), given the input data $U = [u(t_1), u(t_2), \dots, u(t_N)]$ and the sampling positions $X = [x_1, x_2, \dots, x_S]$, the following three assumptions hold.

- 1) There exist integers $N, S > 1$, such that Φ and Y [see (10)] obey the dynamics (5).
- 2) For an arbitrary $\epsilon_1 > 0$, an estimation $\hat{\theta}$ for θ exists such that $\|\hat{\theta} - \theta\| \leq \epsilon_1$.
- 3) For an arbitrary $\epsilon_2 > 0$, the matrix $\hat{\Theta} = \mathcal{C}^{-1}(\hat{\theta})$ has an SVD given in Theorem 3.1 such that $e^{(N_c)} \leq \frac{1}{m_q} \epsilon_2$ with $N_c \leq k$.

Then, the output $\hat{y}(t, x)$ given by (8) with

$$\begin{aligned}\hat{\eta}^{(i)} &= w_i \\ \hat{\xi}^{(i)} &= \sigma_i v_i, \quad i = 1, \dots, N_c\end{aligned}\quad (12)$$

approaches $\bar{y}(t, x)$ of (6) in the sense of

$$\|\hat{y}(t, x) - \bar{y}(t, x)\| \leq \|\phi(z^{-1}, u(t), x)\| \epsilon \quad (13)$$

for $\epsilon = \epsilon_1 + \epsilon_2$.

Proof: Denote

$$\vartheta := \hat{\theta} - \sum_{i=1}^{N_c} \hat{\xi}^{(i)} \otimes \hat{\eta}^{(i)}$$

and

$$\vartheta = [\vartheta_1^T, \vartheta_2^T, \dots, \vartheta_{m_q}^T]^T \in \mathbb{R}^{n_p m_q}, \quad \vartheta_i \in \mathbb{R}^{n_p}.$$

From the definition of $\mathcal{C}(\cdot)$, one has

$$\begin{aligned}\mathcal{C}^{-1}(\vartheta) &= \mathcal{C}^{-1}(\hat{\theta}) - \sum_{i=1}^{N_c} \mathcal{C}^{-1}(\hat{\xi}^{(i)} \otimes \hat{\eta}^{(i)}) \\ &= \hat{\Theta} - \sum_{i=1}^{N_c} \hat{\eta}^{(i)} (\hat{\xi}^{(i)})^T = \hat{\Theta} - \sum_{i=1}^{N_c} \sigma_i w_i v_i^T\end{aligned}$$

and hence

$$\|\mathcal{C}^{-1}(\vartheta)\| = e^{(N_c)} \leq \frac{1}{m_q} \epsilon_2.$$

By the definition of a matrix norm

$$\begin{aligned}\|\mathcal{C}^{-1}(\vartheta)\| &= \sup_{x \neq 0, x \in \mathbb{R}^{mq}} \frac{\|\mathcal{C}^{-1}(\vartheta)x\|}{\|x\|} \\ &= \sup_{x \neq 0, x \in \mathbb{R}^{mq}} \frac{\|[\vartheta_1, \vartheta_2, \dots, \vartheta_{mq}]x\|}{\|x\|} \\ &\geq \|\vartheta_i\|, \quad \forall i = 1, \dots, mq\end{aligned}$$

which implies

$$\|\vartheta\| = \sum_{i=1}^{mq} \|\vartheta_i\| \leq mq \|\mathcal{C}^{-1}(\vartheta)\| \leq \epsilon_2.$$

Next, it is ready to calculate that

$$\begin{aligned}\|\hat{y}(t, x) - \bar{y}(t, x)\| &= \left\| \phi^T(z^{-1}, u(t), x) \left(\sum_{i=1}^{N_c} \hat{\xi}^{(i)} \otimes \hat{\eta}^{(i)} - \theta \right) \right\| \\ &\leq \|\phi^T(z^{-1}, u(t), x)\| \left\| \sum_{i=1}^{N_c} \hat{\xi}^{(i)} \otimes \hat{\eta}^{(i)} - \hat{\theta} + \hat{\theta} - \theta \right\| \\ &\leq \|\phi^T(z^{-1}, u(t), x)\| (\|\vartheta\| + \|\hat{\theta} - \theta\|) \\ &\leq \|\phi^T(z^{-1}, u(t), x)\| (\epsilon_1 + \epsilon_2).\end{aligned}$$

The proof is thus completed. \blacksquare

To achieve a valid estimation $\hat{\theta}$ for θ , we can use the least square estimate (LSE) method [29] as follows:

$$\hat{\theta} = (\Phi^T \Phi)^{-1} \Phi^T Y = \Phi^\dagger Y \quad (14)$$

provided that the inverse $(\Phi^T \Phi)^{-1}$ exists. The LSE approach can almost guarantee a sufficiently small estimation error ϵ_1 in Theorem 3.2. The parameter N_c represents the number of Hammerstein channels. The larger N_c , the smaller $\epsilon_2 = e^{(N_c)} = \sigma_{N_c+1}$ can be selected due to the monotonic order of σ_i . In particular, if $N_c = k$, one can pick $\epsilon_2 = 0$. These observations are summarized in the following corollary.

Corollary 3.1: Let $\hat{\theta}$ calculated by (14) be the LSE of θ in the model (5). Suppose the model (8) [or (9)] is given with (12) for $N_c = k$, and $\hat{\Theta} = \mathcal{C}^{-1}(\hat{\theta})$ has an SVD given in Theorem 3.1. Assume $\|\phi(z^{-1}, u(t), x)\|$ is bounded and the noise $\gamma(t, x)$ is independent of the system input $u(t)$. Then, for any $\varepsilon > 0$, there exist integers $N, S \geq 1$ such that

$$\|\hat{y}(t, x) - \bar{y}(t, x)\| \leq \varepsilon \quad (15)$$

with probability of one, denoted as

$$\hat{y}(t, x) \xrightarrow{a.s.} \bar{y}(t, x). \quad (16)$$

Proof: Let $a \geq 0$ as the bound of $\|\phi(z^{-1}, u(t), x)\|$ and $\epsilon_1 = \varepsilon/a$. Since the external noise $\gamma(t, x)$ is independent of the persistent exciting bounded regressor $\phi(z^{-1}, u(t), x)$, the LSE $\hat{\theta}$ satisfies $\hat{\theta} \xrightarrow{a.s.} \theta$ [29]. That is, there exist integers $N, S \geq 1$ such that

$$\|\hat{\theta} - \theta\| \leq \epsilon_1 \quad (17)$$

with probability of one. As $N_c = k$, one has $\epsilon_2 = mqe^{(N_c)} = 0$ according to the SVD in Theorem 3.1. As a result of Theorem 3.2, one has

$$\|\hat{y}(t, x) - \bar{y}(t, x)\| \leq a(\epsilon_1 + \epsilon_2) = \varepsilon \quad (18)$$

also with probability of one. \blacksquare

Remark 3.1: When $L_i(z^{-1})$ is selected as a stable transfer function, the position x and the input $u(t)$ are bounded, and the functions $\rho_i(x)$, $g_i(u)$, and $\psi_i(x)$ are all bounded, one has a bounded $\|\phi(z^{-1}, u(t), x)\| = \|L(z^{-1}) \otimes \rho(x) \otimes g(u(t)) \otimes \psi(x)\|$.

Remark 3.2: Theorem 3.2 and Corollary 3.1 provide the convergence conditions for the proposed modeling method (14) and (12). By the analysis in Theorem 3.2, the spatial variable x should appear in both the linear block $G(z^{-1}, \cdot)$ and the nonlinear block $N(\cdot)$ of the distributed Hammerstein model, otherwise the convergence and optimality of the present Hammerstein modeling method can not be guaranteed. This claim will also be verified by extensive data-driven modeling experiments of cross couplings on the PI-stage afterwards. Note that Theorem 3.2 holds even in the presence of colored external noises $\gamma(t, x)$, if only it is independent of the input signal $u(t)$. By Theorem 3.2, the required identification channel number (i.e., $\text{rank}(\hat{\Theta}) = k$) can be determined in advance. But, sampling data length should be obtained by applications.

Remark 3.3: The SVD calculation for the proposed multi-channel Hammerstein model is more time consuming than the pseudoinversion calculation of the Preisach model. Accordingly, the convergence time of the former is longer than the latter, but has higher precision, which is beneficial to reduce the positioning control error of multiaxis piezoelectric stages.

Remark 3.4: In the low frequency, typically the linear dynamics part of a piezoelectric system is the dc gain, and the multivalued effect is due to the hysteresis nonlinearity. However, in this work, we present an alternative method to capture the coupled hysteresis and dynamics of piezoelectric actuators with a Hammerstein model. One of the benefits of this development is that the complex hysteresis model is avoided. In this way, both the static nonlinearity and the linear dynamics of the Hammerstein model contribute to describe the hysteresis.

Remark 3.5: Although the cascaded architectures can effectively reduce the X - Y coupling effect, the present parallel architecture in Fig. 2 is irreplaceable due to the following advantages: First, the runout is easily measured and corrected [30]; second, if both axes have the same mechanical bandwidth (like the present case), the testing direction can be chosen arbitrarily [31]. So, it makes sense to investigate the coupling effects. Note that the main contribution of this work lies in the modeling of the coupling effects. Based on our previous control efforts [32], [33] on Hammerstein models, the present work can be expected to extend to controller design. Meanwhile, it is observed from extensive experiments that the cross coupling caused by interaxis friction, pressure, and preload forces have larger effects at lower exciting frequencies.

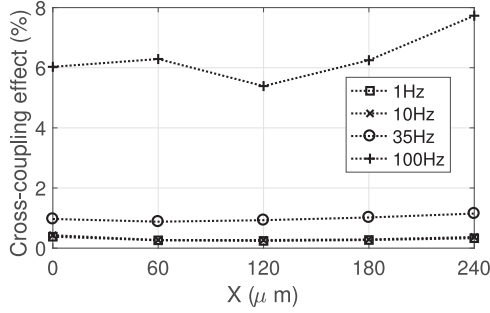


Fig. 5. Evolution of cross-coupling effect at different X - Y axes contacting positions $\{0, 60, 120, 180, 240\}$ μm along the increasing exciting frequency $\{1, 10, 35, 100\}$ Hz. Here, the cross-coupling effect is quantified as the percentage of cross-coupling magnitude to the exciting signal magnitude.

IV. MODELING EXPERIMENTS

First, the PI stage is fed with a periodical exciting voltage signal of $u(t) = 4 + 5 \sin(2\pi ft)$ V with frequency $f \in \{1, 5, 10, \dots, 130\}$ Hz. It is used to describe periodical exciting signals often encountered in real applications. For each integral value of exciting frequency f , we sample NS response signal sequence $y(t, x)$ with $t \in \{t_1, t_2, \dots, t_S\}$, $S = 6000$; $x \in \{x_1, x_2, \dots, x_N\} = \{0, 30, \dots, 240\}$ μm , $N = 9$. Distinct evolution curves of cross-coupling effect are shown in Fig. 5 at different contacting positions $x_i, i = 1, \dots, N$, along increasing exciting frequency f . It is observed that the cross-coupling effect varies at different contacting positions and exciting frequencies. More precisely, the average of the cross-coupling effect percentage at $f \in \{1, 10, 35, 100\}$ Hz are 0.30%, 0.33%, 0.99%, and 6.34%, respectively, which are nonnegligible for high-precision positioning scenarios. Meanwhile, the cross-coupling effect is intensified along increasing exciting frequency.

In the present distributed multichannel Hammerstein model (9), the parameters are picked as follows with $m = 2$, $n = 15$, and $q = p = 8$. In particular, the linear basis series of $L_i(z^{-1})$, $i = 1, 2$, are selected as discrete-time Laguerre basis detailed in Appendix with $\rho = 0.1$ and $T = 2$. Define a set of polynomial and trigonometric functions

$$\mathbb{G} = \{u^i, \sin(ju), \cos(ju) \mid i \in \{0, 1, 2, 3, 7\}, j \in \{1, \dots, 5\}\}.$$

The selection of the nonlinear functions $g_i(u)$, $i = 1, \dots, 15$, makes the complete set \mathbb{G} . The spatial basis functions are picked as polynomials

$$\psi(x) = \rho(x) = [1, x, \dots, x^7]^T.$$

The Hammerstein channel number $N_c = 2$.

Take exciting frequency $f = 10$ Hz, for example, in the first Hammerstein channel, with the aforementioned parameters, the evolution of the coefficient functions $a_i(x) = \psi^T(x)\eta_i^{(1)}$, $i = 1, \dots, 15$, along increasing position x are shown in Fig. 6. It is observed that the magnitudes of coefficients $\{a_1, a_2, a_6, a_{10}, a_{11}\}$ are much greater than the rest, which implies that the formers are more important than the latter. So, to reduce computational complexity and to avoid over-fitting, it suffices to cutoff the unnecessary bases associated to those tiny

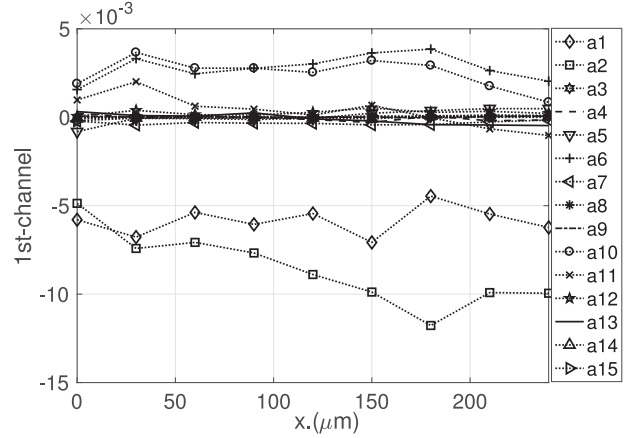


Fig. 6. Spatial-relevant coefficients $a_i(x)$, $i = 1, \dots, 15$, of the first Hammerstein channel of (9).

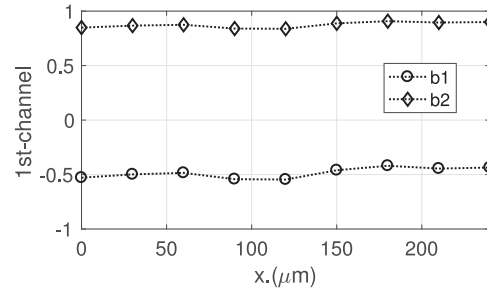


Fig. 7. Spatial-relevant coefficients $b_i(x)$, $i = 1, 2$, of the first Hammerstein model channel of (9).

coefficients. Analogously, the space-relevant coefficient functions $b_i(x) = \rho^T(x)\xi_i^{(1)}$, $i = 1, 2$ in the linear block $G(z^{-1}, x)$ of the first Hammerstein channel are shown in Fig. 7. The spatial distribution of the coefficients of both $N(\cdot, x)$ and $G(z^{-1}, x)$ is thus exhibited, which helps reveal the spatial evolution nature of the nonlinear cross-coupling dynamics.

The X -axis motional modeling performances of $\{0 \mu\text{m}; 1 \text{ Hz}, \dots, 100 \text{ Hz}\}$ and $\{240 \mu\text{m}; 1 \text{ Hz}, \dots, 100 \text{ Hz}\}$ are shown in Fig. 8(a)–(h), respectively. Distinct cross-coupling hysteresis dynamics with different X -positions and exciting frequencies are observed. Again, along with increasing frequency, the cross-coupling effect is intensified, and the nonlinear modeling thus becomes more challenging. Quantitatively speaking, the average magnitude of $\{0 \mu\text{m}; 1 \text{ Hz}, \dots, 100 \text{ Hz}\}$ and $\{240 \mu\text{m}; 1 \text{ Hz}, \dots, 100 \text{ Hz}\}$ are $\{0.98, 1.02, 1.57, 1.36\}$ μm and $\{0.67, 0.80, 1.96, 1.97\}$ μm , respectively. To give a more vivid comparison of the modeling errors at different positions and exciting frequencies, we demonstrate the modeling errors at two contacting points $\{0 \mu\text{m}, 240 \mu\text{m}\}$ along increasing exciting frequencies $\{1 \text{ Hz}, 10 \text{ Hz}, 35 \text{ Hz}, 100 \text{ Hz}\}$. Evidently, the Hammerstein modeling error keeps at a low level (less than 8%), and the effectiveness of the modeling scheme is thus verified. Recall the PI stage resonant frequency of 140 Hz, we set the highest frequency of the exciting input signal as 100 Hz.

Next, to show the merits of the proposed distributed Hammerstein model, we consider the Preisach model [13] as term

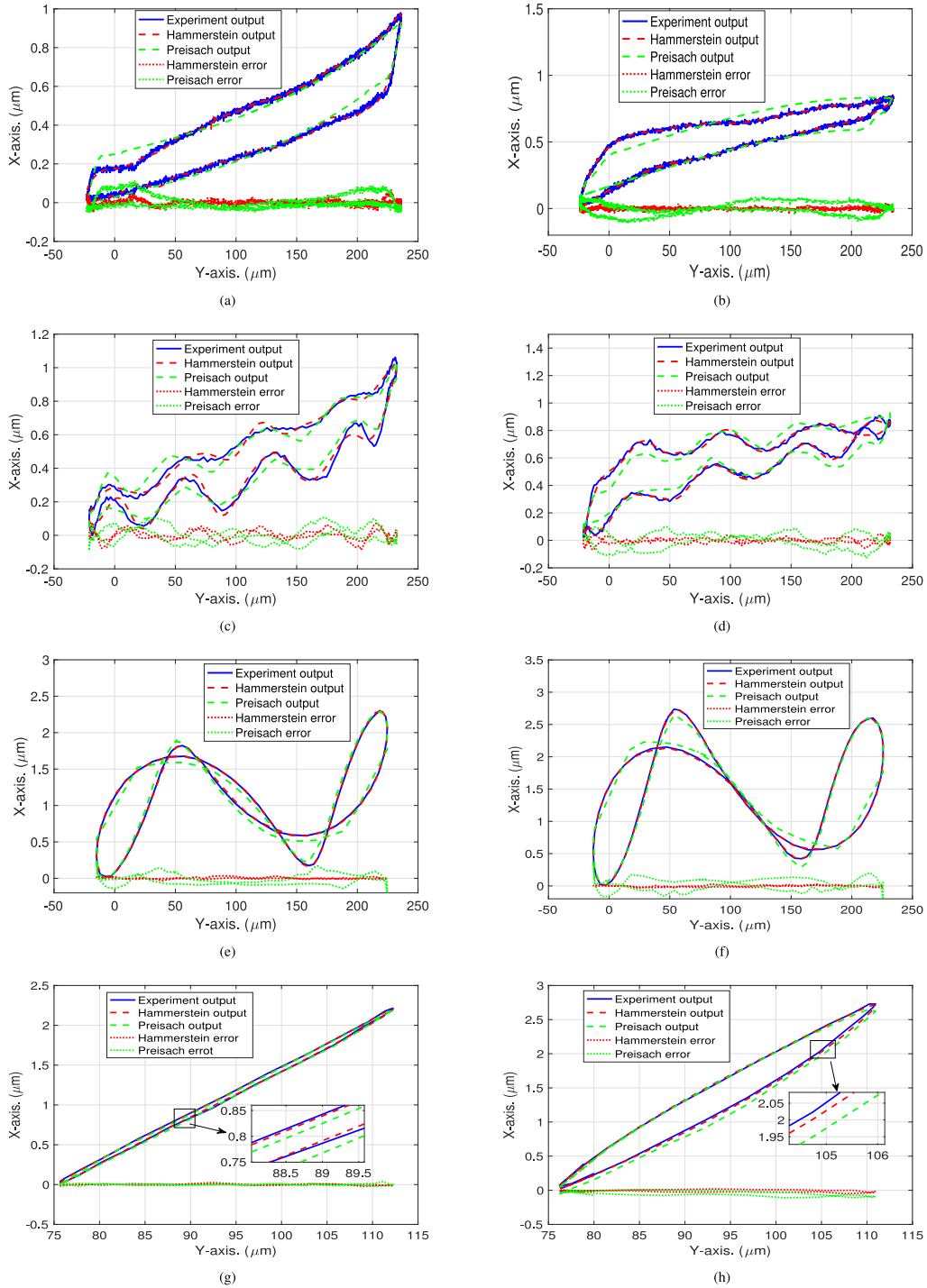


Fig. 8. Modeling performances at X - Y axes contacting positions of $x = 0 \mu\text{m}$ and $x = 240 \mu\text{m}$ with 1 Hz exciting signal are shown in (a) and (b), with 10 Hz in (c) and (d), with 35 Hz in (e) and (f), and with 100 Hz in (g) and (h), respectively.

of comparison in Fig. 8 as well. Due to its asymmetric hysteresis description [34], the modified Preisach model is given in a discrete form as

$$y(k) = p_1 u^3(k) + p_2 u(k) + \sum_{i=1}^n \alpha(r_i) \gamma_i [u(k)] + c \quad (19)$$

where a third-degree polynomial $u(k) + u^3(k)$ is utilized to describe the asymmetric hysteresis, $\gamma_i [u(k)]$ is the play

operator, $n = 10$ is picked as the number of the play operators, $\alpha(r_i) = \ell_i r_i$ is the weighted coefficient of the threshold $r_i = (i - 1)/n$, $i = 1, \dots, n$, and $[p_1, p_2, \alpha(r_1), \dots, \alpha(r_n), c]$ are the coefficient vector. Let $\Omega = [\Omega_1^T, \dots, \Omega_n^T]^T$ with $\Omega_k = [u(k)^3, u(k), \gamma_1 [u(k)], \dots, \gamma_n [u(k)], 1]$ be the input vector, $Y = [y(1), \dots, y(n)]^T$ the output vector, and $X = [p_1, p_2, \alpha(r_1), \dots, \alpha(r_n), c]$ the coefficient vector, so $Y = \Omega X$. Accordingly, the estimated coefficient vector can be calculated as $\hat{X} = (\Omega^T \Omega)^{-1} \Omega^T Y$ by LSE [29].

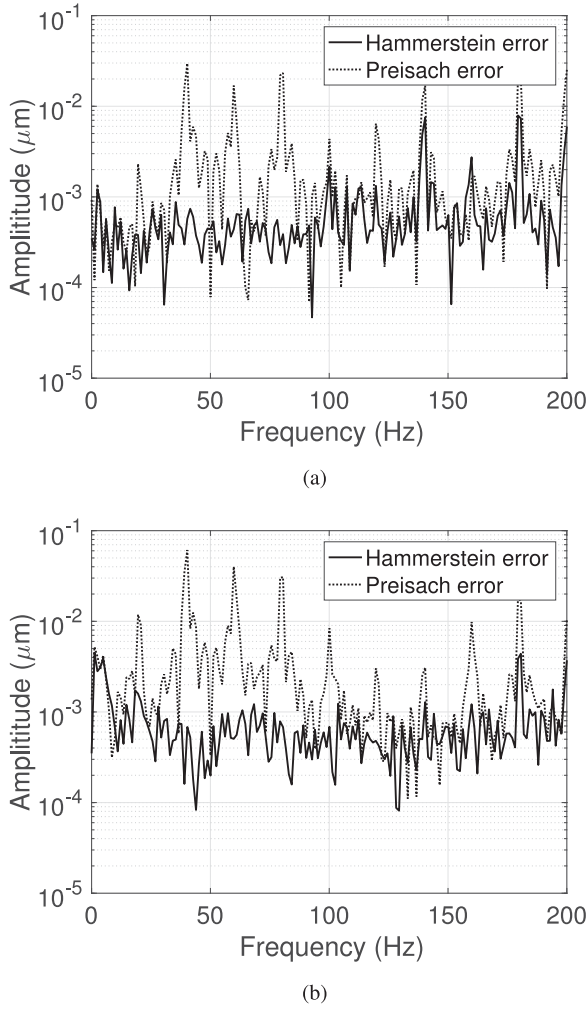


Fig. 9. Spectrum comparison of modeling errors at X–Y axes contacting positions of $x = 0$ and $240 \mu\text{m}$ with $f = 10$ Hz exciting signal are shown in (a) and (b), corresponding to Fig. 8(c) and (d), respectively.

Evidently, it is observed in Fig. 8 that the modeling error of the present Hammerstein model is much lower than that of the Preisach model. Meanwhile, with increasing exciting frequency, the modeling accuracy advantage of Hammerstein model is intensified. To show the result more vividly, we exhibit the modeling errors of the two models, respectively, in frequency domain in Fig. 9 with $f = 10$ Hz. It is observed that the modeling error e of the proposed Hammerstein model is much lower than that of the Preisach model within the entire bandwidth of $[0, 300]$ Hz, especially within the bandwidth of $[25, 100]$ Hz. To make a quantitative comparison between the two models, we exhibit the modeling errors of the Hammerstein and Preisach models in Fig. 10 with different exciting frequencies and X–Y axes contacting positions. Therein, compared with the Preisach model, the average modeling error of the Hammerstein model with exciting frequency $f = \{1, 10, 35, 100\}$ Hz has been decreased by $\{52\%, 62\%, 74\%, 55\%\}$, respectively. Especially, the scenarios of 1 and 100 Hz are shown in Fig. 10(a) and (b), respectively. Here, the modeling error is calculated as $e(t, x) := \frac{y(t, x) - y_m(t, x)}{y_{\text{max}}(t, x) - y_{\text{min}}(t, x)}$, the average modeling error $e(x)$

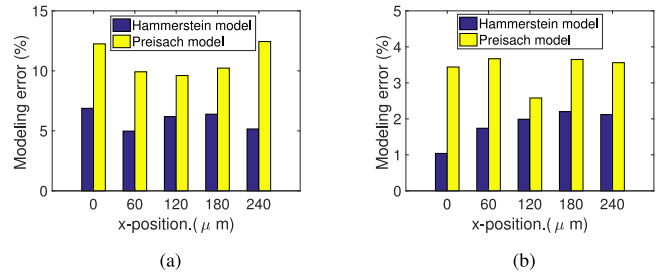


Fig. 10. Modeling errors of distributed Hammerstein model and Preisach model at different X–Y axes contacting positions with 1 Hz exciting input signal are shown in (a), and with 100 Hz in (b), respectively.

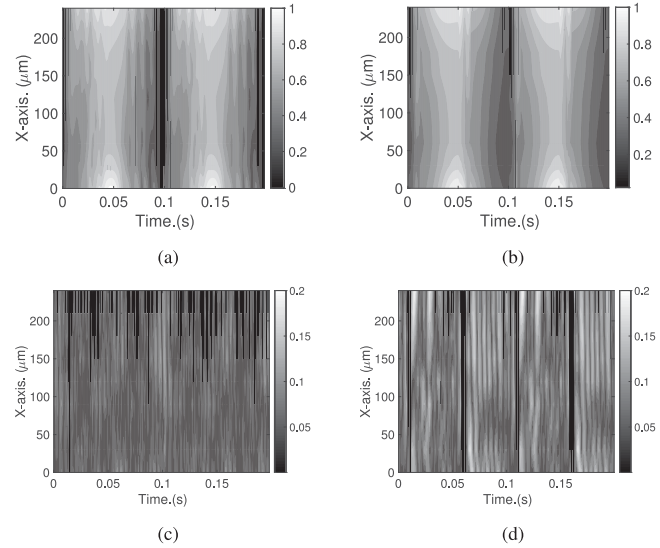


Fig. 11. (a), (b) Output heat maps of the Hammerstein and Preisach models of the cross-coupling effect, respectively. (c), (d) Error heat maps of the Hammerstein and Preisach models, respectively.

is the average of $e(t, x)$ over time t , and the average modeling error e at each exciting frequency f is the average of $e(x)$ over positions x . The effectiveness and superiority of the presented distributed Hammerstein method are thus verified. The advantage of the proposed Hammerstein model lies in its approximating capacity of both the nonlinearity and the spatial distribution of the cross-coupling effect. Note that, since the Preisach model does not effectively work with exciting frequency $f = 35$ Hz, we just show the modeling curve of Hammerstein model in Fig. 8(e) and (f). Moreover, since interaxis friction is intensified along rising excitation signal frequency, the coupling effect increases as well. Besides, the 100 Hz coupling hysteresis in Fig. 8(g) and (h) are more symmetric than the 1 Hz one in Fig. 8(a) and (b). Due to the symmetry of the Preisach operators, the modeling errors of the former is smaller than the latter. It is still worth mentioning that, to avoid over/less fitting, the series lengths of both linear and nonlinear blocks should be tuned according to the real sampling data.

To put the cross-coupling investigation into a more general scenario, we demonstrate the spatial/temporal evolution of the cross coupling along increasing spatial variable x and temporal variable t in Fig. 11. Therein, we use an exciting input signal

$u(t) = 4 + 5 \sin(2\pi ft)$ V with $f = 1$ and 100 Hz, respectively. It is observed that the modeling error of the distributed Hammerstein model ($\leq 8\%$ for $f = 1$ Hz, and $\leq 2.2\%$ for $f = 100$ Hz) is much less than that of the Preisach model ($\leq 13\%$ for $f = 1$ Hz, and $\leq 3.8\%$ for $f = 100$ Hz). The general virtue of the proposed distributed Hammerstein model is thus further verified.

V. CONCLUSION

Cross coupling has nonnegligible adverse effects on the positioning control precision of multiaxis piezoelectric micropositioning stages, which hinders their further applications to nanoprecision detection and manufacturing systems. In this paper, a distributed multichannel Hammerstein model is proposed to approximate the spatial/temporal evolution of the nonlinear dynamics of the cross-coupling hysteresis. Theoretical analysis is provided to guarantee the convergence and modeling accuracy of the proposed distributed Hammerstein model. Finally, extensive modeling experiments are conducted to show its feasibility and superiority.

APPENDIX

The selection of $L(z^{-1}) = [L_1(z^{-1})^T, \dots, L_m(z^{-1})^T]^T$ follows the Laguerre functions given in [35] and [36]. A slight abuse of notation of mixing time domain signals and frequency domain transfer function is used in Section III. Indeed, the real implementation of $\zeta(t) = L(z^{-1})\mu(t)$ is given by the following dynamic equation in time domain

$$\zeta(t+1) = A\zeta(t) + B\mu(t)$$

where, for two parameters ϱ and T ,

$$A = \begin{bmatrix} \rho_1 & 0 & \dots & 0 \\ \frac{-\rho_1\rho_2 - \rho_3}{T} & \rho_1 & \dots & 0 \\ \vdots & \ddots & \ddots & \vdots \\ \frac{(-1)^{m-1}\rho_2^{m-2}(\rho_1\rho_2 + \rho_3)}{T^{m-1}} & \dots & \frac{-\rho_1\rho_2 - \rho_3}{T} & \rho_1 \end{bmatrix}$$

$$B = \left[\rho_4 \left(\frac{-\rho_2}{T} \right) \rho_4 \dots \left(\frac{-\rho_2}{T} \right)^{m-1} \rho_4 \right]^T$$

and

$$\rho_1 = \exp(-\varrho T), \quad \rho_2 = T + \frac{2}{\varrho}(\rho_1 - 1)$$

$$\rho_3 = -T\rho_1 - \frac{2}{\varrho}(\rho_1 - 1), \quad \rho_4 = \sqrt{2p} \frac{1 - \rho_1}{\varrho}.$$

REFERENCES

- [1] G. Binnig and H. Rohrer, "Scanning tunneling microscopy," *Surface Sci.*, vol. 126, no. 1–3, pp. 236–244, 1983.
- [2] G. Binnig, C. F. Quate, and C. Gerber, "Atomic force microscope," *Phys. Rev. Lett.*, vol. 56, no. 9, pp. 930–933, 1986.
- [3] A. Tay, W. K. Ho, and X. Wu, "Real-time control of photoresist extinction coefficient uniformity in the microlithography process," *IEEE Trans. Control Syst. Technol.*, vol. 15, no. 1, pp. 99–105, Jan. 2007.
- [4] Y. Yamagata and T. Higuchi, "Ultrahigh vacuum precise positioning device utilizing rapid deformations of piezoelectric elements," *J. Vac. Sci. Technol.*, vol. 1, no. 8, pp. 89–91, 1990.
- [5] R. Fukui, A. Torii, and A. Ueda, "Robot actuated by rapid deformation of piezoelectric elements," in *Proc. Int. Symp. Micromechatronics Human Sci.*, 2001, pp. 117–122.
- [6] G.-Y. Gu, L.-M. Zhu, C.-Y. Su, H. Ding, and S. Fatikow, "Modeling and control of piezo-actuated nanopositioning stages: A survey," *IEEE Trans. Autom. Sci. Eng.*, vol. 13, no. 1, pp. 313–332, Jan. 2016.
- [7] Y. K. Yong, S. R. Moheimani, B. J. Kenton, and K. K. Leang, "High-speed flexure-guided nanopositioning: Mechanical design and control issues," *Rev. Sci. Instrum.*, vol. 83, no. 12, 2012, Art. no. 121101.
- [8] S. Karunanidhi and M. Singaperumal, "Design, analysis and simulation of magnetostrictive actuator and its application to high dynamic servo valve," *Sens. Actuators A, Phys.*, vol. 157, no. 2, pp. 185–197, 2010.
- [9] Y. K. Yong, K. Liu, and S. O. R. Moheimani, "Reducing cross-coupling in a compliant XY nanopositioner for fast and accurate raster scanning," *IEEE Trans. Control Syst. Technol.*, vol. 18, no. 5, pp. 1172–1179, Sep. 2010.
- [10] Y. Sun and J. H. L. Pang, "AFM image reconstruction for deformation measurements by digital image correlation," *Nanotechnology*, vol. 17, no. 4, pp. 933–939, 2006.
- [11] Habibullah, H. R. Pota, I. R. Petersen, and M. S. Rana, "Creep, hysteresis, and cross-coupling reduction in the high-precision positioning of the piezoelectric scanner stage of an atomic force microscope," *IEEE Trans. Nanotechnol.*, vol. 12, no. 6, pp. 1125–1134, Nov. 2013.
- [12] O. M. E. Rifai and K. Youcef-Toumi, "Coupling in piezoelectric tube scanners used in scanning probe microscopes," in *Proc. Amer. Control Conf.*, 2001, vol. 4, pp. 3251–3255.
- [13] P. Ge and M. Jouaneh, "Generalized Preisach model for hysteresis nonlinearity of piezoceramic actuators," *Precis. Eng.*, vol. 20, no. 2, pp. 99–111, 1997.
- [14] R. Bouc, "Forced vibration of mechanical systems with hysteresis," in *Proc. Conf. Nonlinear Oscillation, Prague*, 1967, pp. 32–39.
- [15] M. Goldfarb and N. Celanovic, "Modeling piezoelectric stack actuators for control of micromanipulation," *IEEE Trans. Control Syst. Technol.*, vol. 17, no. 3, pp. 69–79, Jun. 1997.
- [16] J.-W. Wu, J.-J. Chen, M.-L. Chiang, J.-T. Yu, and L.-C. Fu, "Design and control of phase-detection mode atomic force microscopy for reconstruction of cell contours in three dimensions," *IEEE Trans. Nanotechnol.*, vol. 13, no. 4, pp. 639–649, Jul. 2014.
- [17] M. S. Rana, H. R. Pota, and I. R. Petersen, "Nonlinearity effects reduction of an AFM piezoelectric tube scanner using MIMO MPC," *IEEE/ASME Trans. Mechatronics*, vol. 20, no. 3, pp. 1458–1469, Jun. 2015.
- [18] Y.-Q. Xie, Y.-H. Tan, and R.-L. Dong, "Nonlinear modeling and decoupling control of XY micropositioning stages with piezoelectric actuators," *IEEE/ASME Trans. Mechatronics*, vol. 18, no. 3, pp. 821–832, Jun. 2013.
- [19] Y.-D. Qin, B. Shirinzadeh, Y.-L. Tian, L. Yan, D.-W. Zhang, and U. Bhagat, "Design and computational optimization of a decoupled 2-DOF monolithic mechanism," *IEEE/ASME Trans. Mechatronics*, vol. 19, no. 3, pp. 872–881, Jun. 2014.
- [20] U. Bhagat, B. Shirinzadeh, L. Clark, Y.-D. Qin, Y.-L. Tian, and D.-W. Zhang, "Experimental investigation of robust motion tracking control for a 2-DOF flexure-based mechanism," *IEEE/ASME Trans. Mechatronics*, vol. 19, no. 6, pp. 1737–1745, Dec. 2014.
- [21] R.-F. Fung, Y.-L. Hsu, and M.-S. Huang, "System identification of a dual-stage XY precision positioning table," *Precis. Eng.*, vol. 33, pp. 71–80, 2009.
- [22] S. K. Das, H. R. Pota, and I. R. Petersen, "Multivariable negative-imaginary controller design for damping and cross coupling reduction of nanopositioners: A reference model matching approach," *IEEE/ASME Trans. Mechatronics*, vol. 20, no. 6, pp. 3123–3134, Dec. 2015.
- [23] Q. Xu, "Identification and compensation of piezoelectric hysteresis without modeling hysteresis inverse," *IEEE Trans. Ind. Electron.*, vol. 60, no. 9, pp. 3927–3937, Sep. 2013.
- [24] C. Qi, H.-T. Zhang, and H.-X. Li, "A multi-channel spatio-temporal Hammerstein modeling approach for nonlinear distributed parameter processes," *J. Process Control*, vol. 19, pp. 85–99, 2009.
- [25] C.-X. Li, G.-Y. Gu, M.-J. Yang, and L.-M. Zhu, "Design, analysis and testing of a parallel-kinematic high-bandwidth XY nanopositioning stage," *Rev. Sci. Instruments*, vol. 84, no. 12, 2013, Art. no. 125111.

[26] L.-J. Lai, G.-Y. Gu, and L.-M. Zhu, "Design and control of a decoupled two degree of freedom translational parallel micro-positioning stage," *Rev. Sci. Instruments*, vol. 83, no. 4, 2012, Art. no. 045105.

[27] P. Duren, *Theory of Hp-Spaces*. New York, NY, USA: Academic, 1970.

[28] G. H. Golub and C. F. V. Loan, *Matrix Computations*, 3rd ed. Baltimore, MD, USA: The Johns Hopkins Univ. Press, 1996.

[29] L. Ljung, *System Identification*, 2nd ed. Englewood Cliffs, NJ, USA: Prentice-Hall, 1999.

[30] Y. Li and Q. Xu, "Design and analysis of a totally decoupled flexure-based XY parallel micromanipulator," *IEEE Trans. Robot.*, vol. 25, no. 3, pp. 645–657, Jun. 2009.

[31] G. Schitter, P. J. Thurner, and P. K. Hansma, "Design and input-shaping control of a novel scanner for high-speed atomic force microscopy," *Mechatronics*, vol. 18, no. 5–6, pp. 282–288, 2008.

[32] G.-Y. Gu, C.-X. Li, L.-M. Zhu, and C.-Y. Su, "Modeling and identification of piezoelectric-actuated stages cascading hysteresis nonlinearity with linear dynamics," *IEEE/ASME Trans. Mechatronics*, vol. 21, no. 3, pp. 1792–1797, Jun. 2016.

[33] C.-X. Li, G.-Y. Gu, L.-M. Zhu, and C.-Y. Su, "Odd-harmonic repetitive control for high-speed raster scanning of piezo-actuated nanopositioning stages with hysteresis nonlinearity," *Sens. Actuators: A, Phys.*, vol. 244, pp. 95–105, 2016.

[34] G.-Y. Gu, L.-M. Zhu, and C.-Y. Su, "Modeling and compensation of asymmetric hysteresis nonlinearity for piezoceramic actuators with a modified Prandtl–Ishlinskii model," *IEEE Trans. Ind. Electron.*, vol. 61, no. 3, pp. 1583–1595, Mar. 2014.

[35] C. C. Zervos and G. A. Dumont, "Deterministic adaptive control based on Laguerre series representation," *Int. J. Control*, vol. 48, no. 6, pp. 2333–2359, 1988.

[36] G. A. Dumont, C. C. Zervos, and G. L. Pageau, "Laguerre-based adaptive control of pH in an industrial bleach plant extraction stage," *Automatica*, vol. 26, no. 4, pp. 781–787, 1990.



Zhiyong Chen (S'03–SM'13) received the B.E. degree in automation from the University of Science and Technology of China, Hefei, China, and the M.Phil. and Ph.D. degrees in automation from the Chinese University of Hong Kong, Hong Kong, in 2000, 2002, and 2005, respectively.

During 2005–2006, he was a Research Associate with the University of Virginia. In 2006, he joined the University of Newcastle, Callaghan, NSW, Australia, where he is currently a Professor. He is also a Changjiang Chair Professor with Central South University, Changsha, China. His research interests include nonlinear systems and control, biological systems, and multiagent systems. He is/was an Associate Editor for *Automatica*, IEEE TRANSACTIONS ON AUTOMATIC CONTROL, and IEEE TRANSACTIONS ON CYBERNETICS.



Dongrui Wu (S'05–M'09–SM'14) received the Ph.D. degree in electrical engineering from the University of Southern California, Los Angeles, CA, USA, in 2009.

He was a Lead Researcher with GE Global Research, and Chief Scientist of several startups. He is currently a Professor with the School of Automation, Huazhong University of Science and Technology, Wuhan, China. His research interests include affective computing, brain-computer interface, computational intelligence,

and machine learning.

Dr. Wu is an Associate Editor for the IEEE TRANSACTIONS ON FUZZY SYSTEMS, IEEE TRANSACTIONS ON HUMAN-MACHINE SYSTEMS, and the IEEE COMPUTATIONAL INTELLIGENCE MAGAZINE. He was the recipient of the IEEE CIS Outstanding Ph.D. Dissertation Award in 2012, and the IEEE Transactions on Fuzzy Systems Outstanding Paper Award in 2014.



Hai-Tao Zhang (M'07–SM'13) received the B.E. and Ph.D. degrees in automation from the University of Science and Technology of China, Hefei, China, in 2000 and 2005, respectively.

During January–December 2007, he was a Postdoctoral Researcher with the University of Cambridge, Cambridge, U.K. Since 2005, he has been with Huazhong University of Science and Technology, Wuhan, China, where he was an Associate Professor from 2005 to 2010 and has been a Full Professor since 2010. His re-

search interests include swarming intelligence, model predictive control, and multiagent systems control.

Dr. Zhang is an Associate Editor for IEEE TRANSACTIONS ON CIRCUITS AND SYSTEMS II and *Asian Journal of Control*.



Bo Hu received the Bachelor's degree in automation from Hefei University of Technology, Hefei, China, in 2015, and the Master's degree in engineering from Huazhong University of Science and Technology, Wuhan, China, in 2017.

His research interests include nonlinear hysteresis modeling and control.



Linlin Li received the B.E. degree (with Hons.) in mechanical design, manufacturing, and automation from Shandong University, Jinan, China, in 2014. She is currently working toward the Ph.D. degree in mechanical engineering at Shanghai Jiao Tong University, Shanghai, China.

Her research interests include mechatronics, modeling and control of high-bandwidth nanopositioning stages, and atomic force microscope.



Bowen Xu received the B.S. degree in automation from Xidian University, Xi'an, China, in 2016. He is currently working toward the Ph.D. degree in automation at the School of Automation, Huazhong University of Science and Technology, Wuhan, China.

His current research focuses on multiagent systems control.

Mr. Xu was an outstanding Reviewer for *Asian Journal of Control* in 2017.



Xiang Huang received the B.S. degree in automation from Wuhan University of Science and Technology, Wuhan, China, in 2015. He is currently working toward the Ph.D. degree in automation at the School of Automation, Huazhong University of Science and Technology, Wuhan, China.

His research interests include modeling and control of hysteresis.



Guoying Gu (S'10–M'13) received the B.E. degree in electronic science and technology from Shanghai Jiao Tong University, Shanghai, China, in 2006 and Ph.D. degree in mechatronic engineering from Shanghai Jiao Tong University, Shanghai, China, in 2012, respectively.

Since October 2012, he has been with Shanghai Jiao Tong University, where he is currently a Professor. He was a Humboldt Postdoc Fellow with the University of Oldenburg, Oldenburg, Germany. He was a Visiting Scholar with

the Massachusetts Institute of Technology, the National University of Singapore, and the Concordia University. His research interests include soft robotics, bioinspired robot design and motion control, smart materials actuators and sensors, and additive manufacturing with soft materials.

Dr. Gu is the recipient of multiple awards, including Young Changjiang Scholar of the Chinese Ministry of Education, National Science Fund for Excellent Young Scholars, and the first prize of Natural Science of Ministry of Education. He is currently an Associate Editor for *International Journal of Advanced Robotic Systems*.



Ye Yuan (M'13) received the B.Eng. degree (Valedictorian) in automation from the Department of Automation, Shanghai Jiao Tong University, Shanghai, China, in 2008, and the M.Phil. and Ph.D. degrees in engineering from the Department of Engineering, University of Cambridge, Cambridge, U.K., in 2009 and 2012, respectively.

Since 2016, he has been a Full Professor with Huazhong University of Science and Technology, Wuhan, China. Prior to this, he was a Postdoctoral Researcher with UC Berkeley, a Junior Research Fellow with Darwin College, University of Cambridge. His research interests include system identification and control with applications to cyber-physical systems.

Dr. Yuan has received the China National Recruitment Program of 1000 Talented Young Scholars, the Dorothy Hodgkin Postgraduate Awards, Microsoft Research Ph.D. Scholarship, Best of the Best Paper Award at the IEEE PES General Meeting, Best Paper Finalist at the IEEE International Conference on Information and Automation.